The representation of Gravity Waves in Atmospheric General Circulation Models (GCMs)

François Lott [1]
and Christophe Millet [2]

Version du 10 Juillet 2008,

En préparation pour
Infrasound monitoring for atmospheric studies

Abstract

A potential long-term application of infrasound detection is related to the fact that nonlinear mountain flow dynamics and breaking gravity waves in the high atmosphere produce infrasounds, and/or affect the propagation of the infrasounds. In the future, we can imagine that the compressible models developed in meteorology will permit to links these mesoscale meteorological events to the infrasounds they produce. Nowadays, the parameterization of gravity waves in Numerical Weather Prediction models (NWP) and General Circulation Models (GCM) could also be used to predict the places where the infrasounds are produced.

The paper here does not adress these issues specifically, but recall that nonlinear mountain flow dynamics and breaking gravity waves are very significant for the Atmospheric Climate. To establish this, we discuss how these effects are represented in General Circulation Models (GCMs), and wich impacts they have on the climate of these models.

First is presented a subgrid-scale orographic drag scheme that includes both gravity waves drag and low-level drag that are based on well-understood mesoscale mountain flow dynamics. Second is presented the non-orographic gravity waves drag schemes used in most GCMs that include a middle atmosphere. The impacts of these different schemes on the LMDz-GCM extended to the middle atmosphere are detailed.

[1]Laboratoire de Météorologie Dynamique, Ecole Normale Supérieure, 24 rue Lhomond, 75231 Paris Cedex 05, France. flott@lmd.ens.fr

[2]Laboratoire de Détection et de Géophysique, CEA DAM Ile de France, Bruyères-le-Châtel, 91297 Arpajon Cedex, France. christophe.millet@cea.fr

1 Introduction

To monitor nuclear explosions, it is necessary to model the long-range propagation of low-frequency acoustic (infrasonic) waves through the atmosphere. The infrasound propagation models used for this purpose are still based on asymptotic methods like the ray tracing techniques, the normal mode approach, and the resolution of the parabolic equation. These techniques cannot explain some important signals in the microbarograph measurements (Millet et al. 2007, Ponomarev et al. 2006 and Kulichkov et al. 2004, 2002). Actually, the vertical scales of the low waveguide modes involved in the long-range propagation of infrasounds are comparable with the vertical scales of the atmospheric motions due to the internal gravity waves. Furthermore, these methods also assume that the atmospheric flow varies slowly in time compared to the infrasound time-scale. This is again not true in the presence of gravity waves.

To circumvent these difficulties, the future generation of infrasound propagation models will be based on the resolution of the primitive equations of motion. The most recent models become similar as the present Numerical Weather Forecasting Models (NWP) and the climate models, except that they include compressible effects[3]. Based on suitable numerical schemes, these models are able to capture acoustic waves as well as gravity waves, but still fail to compute wave motions in the same way as atmospheric motions. For instance, one of the common issues deals with the treatment of radiation and outflow boundary conditions, whereas a simple rigid, free-slip surface is often employed in NWP models.

Internal Gravity Waves (GWs) are ubiquitous in the atmosphere. They are observed for instance by the high-resolution radiosondes, which give vertical profiles of temperature and velocity (e.g., Dalaudier et al. 1994). Although gravity waves are quite coherent and predictible when they are produced by mountains, they are much more random when they are caused by other sources (convection, geostrophic adjustment in fronts, shear instabilities). This becomes particularly true in the middle atmosphere where the influence of waves coming from various independent sources can be felt at the same place. In this case, a statistical description is more adapted, and many measurements have shown that the GWs spectra in the vertical direction follow a spectral law given by $E \sim N^2 m^{-3}$, where E, N and m are respectively the kinetic or potential energy (expressed per unit mass), the Brunt-Väisälä frequency and the vertical wavenumber. These spectra are observed in the range of vertical wavelengths $2\pi/m$ between 100 m and few kilometers. When they break, which generally occur when $2\pi/m < 100$ m, the turbulence results in Kolmogoroff spectra. As these spectra are quite universal,

[3]For completeness note that the NWP models still adopt approximations or numerical techniques that filter out a good fraction of the sound waves

most parameterizations of the non-orographic GW in General Circulation Models are based on them (Hines 1997, Warner & McIntyre 1996). This make them quite different from the parameterization of the mountain gravity waves, which use their more predictive nature (Lott and Miller 1997).

In General Circulation Models, quite substantial systematic errors have been reduced by including the parameterizations of orographic and non-orographic gravity waves. Historically, the orographic GWs routines have been introduced during the mid-eighties, when the global GCMs where limited to the troposphere and lower stratosphere resolution (Palmer et al. 1986). The non-orographic routines are more recent, and have been introduced when the GCMs have begun to extent up to the mesosphere (Manzini et al. 1997). Such routines permit to correct the zonal mean wind and the zonal mean temperature at the summer mesopause.

The parameterization of mountain gravity waves alleviates systematic errors in GCM simulations of the tropospheric westerlies (Palmer et al., 1986). Miller et al. (1989) extended this study, showing that the representation of orography in global models have an impact (positive or negative) on many of the large scale structures mentioned before. Miller et al. (1989) and also Stephenson (1994) have shown that the vertical repartition of the mountain drag is an important issue for GCMs. These large scale simulations obviously provide important applications for the 2-D (Clark and Peltier, 1984; Durran, 1987) and 3-D (Miranda and James, 1992; Schär and Durran, 1996) theoretical studies on mountain flow. Following these, Lott and Miller (1997) (hereafter LM97) have proposed a Subgrid Scale Orographic (SSO) drag scheme which gives particular attention to the drag of the flow at levels that intersect the subgrid-scale orography. These scheme is also validated against the PYREX data (Bougeault et al., 1993) in all the situations for which the incident wind perpendicular to the ridge is strong.

Among the quasi-steady patterns that SSO parameterization schemes affect, the steady planetary wave is of particular interest because its simulation is rather difficult. For instance, Fig. A1 in D'Andrea et al. (1996) shows the steady geopotential height field for 15 different models: among them, many (but not all) are too zonal. To correct these errors one has to determine which processes related to the mountains, contribute to the steady planetary wave. For this purpose the quasi geostrophic models are helpful because they have been extensively used in diagnosing the forcing of planetary waves (Held 1983). In these models, mountains induce vortex stretching, modifying the vorticity, but keeping the potential vorticity unchanged. Interestingly, the circulation over mountains associated to vortex stretching, is driven by a force whose horizontal component is perpendicular to the incident flow in the linear quasi-geostrophic context and that is proportional to the mountain volume (Smith, 1979). In the context of atmospheric models which do not use the quasi geostrophic approximation, the fact that vortex stretching

can be eventually accounted for by a force which is quite predictable was used in Lott (1999) to reduce errors on the model simulation of the planetary waves.

Because this book is devoted to surface process, the recent progresses in developing new gravity wave drag schemes, that include non-orographic waves are only mentioned here briefly and for completeness. Detailed impacts of such a scheme are nevertheless given in the Section 3.2. The need for such schemes follow that most GCMs now extend to the middle atmosphere, where the circulation is largely controlled by wave-induced forces (Rossby and Gravity waves) (Holton et al. 1995; Haynes et al. 1995). For the gravity wave part and in summer, mountain waves can not provide these forces, because they have good chances to encounter critical levels in the low stratosphere (Lindzen 1981). Furthermore, the forces needed in this season and near the mesopause are opposite in sign with the forces mountain waves can provide. Finally, observations suggest that steady gravity waves are seldom above about 20 km altitude. The general way non-orographic drag scheme are developed is grossly presented in Section 3, together with some results obtained in the LMD-GCM extended to the middle atmosphere, and including the Hines (1997) parameterization scheme tested by Manzini et al. (1997) in the ECHAM4 model.

2 The different parameterizations

2.1 Subgrid-scale orographic drag

The orographic drag scheme presented here is adapted from LM97 and used in Lott (1998). The SSO over one gridpoint region is represented by seven parameters, μ, γ, σ, θ, Z_{min}, Z_{max} and Z_{mea} which stand for the standard deviation, the anisotropy, the slope, the orientation, the minimum, the maximum and the mean elevation of the orography respectively. These seven parameters are evaluated over a grid point region from the US Navy dataset (on 10×10 degree grids). The scheme uses values of low-level wind and static stability which are partitioned into two parts. The first corresponds to the incident flow, and is evaluated by averaging the wind, the Brunt-Väisälä frequency and the fluid density between the model ground Z_o and the mountain peaks Z_{max}. This low-level flow is referenced as $\mathbf{U_H}$, N_H and ρ_H, respectively. The second part is the "blocked" flow, whose upper height Z_b, is the highest level that satisfies the condition,

$$\int_Z^{Z_{max}} \frac{N}{U_p} dz \leq H_{NC} \ , \tag{1}$$

where the wind speed $U_p(z)$ is calculated by resolving the wind $\mathbf{U}$ in the direction of the incident flow $\mathbf{U_H}$. The parameter H_{NC} tunes the depth of the blocked flow layer and is of order one. Then, for each layer below Z_b a force per unit volume is applied:

$$\mathbf{D_b}(z) \;=\; -\rho C_d \max\left(2-\frac{1}{r}\;,\;0\right)\frac{\sigma}{2\mu}\left(\frac{Z_b-z}{Z_b-Z_o}\right)(B\cos^2\psi + C sin^2\psi)\frac{\mathbf{U}|\mathbf{U}|}{2}\;. \quad (2)$$

In Eq. (2) the angle between the incident flow and the normal ridge direction is ψ, the aspect ratio of the obstacle as seen by the incident flow is r. The functions $B(\gamma)$ and $C(\gamma)$ are of order 1 and take into account the anisotropy of the SSO (see LM97). The parameter C_d, which is typically of order unity from the literature on flow dynamics around bluff body, tunes the blocked flow drag amplitude.

On the supposition that when there is low-level flow blocking, the effective height of the SSO felt by the fluid is reduced to $Z_{max} - Z_b$, the gravity wave stress (i.e., force per unit area) is reduced accordingly. It becomes after evaluation of the typical number of ridges within a grid point region,

$$\tau \;=\; \rho_H G U_H N_H \left(Z_{max}-Z_b\right)^2 \frac{\sigma}{4\mu}\left(B\cos^2\psi_H + C\sin^2\psi_H; (B-C)\sin\psi_H\cos\psi_H\right) \quad (3)$$

The parameter G tunes the gravity waves stress amplitude, and is also of order 1. The vertical repartition of the gravity wave stress determines the levels at which the waves are dissipated and slow down the mean flow. First, the stress decays by a tunable factor $\beta < 1$, between the ground and the 850hPa level to crudely account for the low-level dissipation of the trapped lee waves (see Miller et al. (1989) and the Appendix). Above, breaking occurs when the total Richardson number Ri falls below a critical value Ri_c which is of order unity.

2.2 Orographic lift

In the model itself, the lift representation consists of applying a force per unit volume $\mathbf{L}$ that is perpendicular to the wind at each levels below the mountain maximum height Z_{max}

$$\mathbf{L} \;=\; -\,\rho\, C_l\, f\left(\frac{Z_{max}-Z}{Z_{max}-Z_o}\right)\,\mathbf{k}\times\mathbf{u}\,. \quad (4)$$

In Eq. (4), f is the Coriolis frequency, and C_l is a tunable parameter of order 1. When the incident wind is uniform in the vertical, Eq. (4) integrated from the model ground Z_o to the mountain peak Z_{max} gives a stress,

$$\mathcal{L} \;=\; -\,\rho\, C_l\, f\left(\frac{Z_{max}-Z_o}{2}\right)\,\mathbf{k}\times\mathbf{u}\,. \quad (5)$$

which is near the lift stress exerted by an obstacle on a quasi-geostrophic flow (Smith, 1979).

2.3 Non-orographic waves

Because the non-orographic schemes include ensemble of waves with far different propagation properties, a convenient way to formulate them is to adopt a spectral representation. These differentiate them fundamentally from most current orographic schemes, where a representation in the physical space is necessary at low level, to account for non-linearities. For mountain waves, the description in the physical space remains adequate aloft, providing the waves are hydrostatic. For non-orographic waves the spectral representation is also motivated by that numerous observational studies, suggest that gravity waves energy spectra have a slope at large vertical wavenumber m that is roughly independent of time and position.

Practical GWs spectral gravity waves parameterization schemes (see for instance Hines 1997; Warner and Mc Intyre 1996, 2001) tend to describe gravity wave spectral evolution in terms of the vertical propagation and saturation of a spectrum, that is imposed at a given launch altitude. A good example of such a scheme is that of Warner and Mc Intyre (1996), where the evolution of the spectra from one altitude to the next, is based on well understood aspects of linear conservative gravity waves propagation. The saturation is then entirely empirical. When the spectra transported conservatively, present in the vertical wavenumber space, a saturated portion (i.e. the portion at 'large' m) that exceed a given threshold, this threshold is imposed as the knew spectra. To fit data, this threshold can include the m^{-3} slope suggested by observations. For historical reasons, in the LMD-GCM we have used until now the scheme proposed by Hines (1997), which try to include more sophisticated wave breaking models. In practice nevertheless, it is likely that the schemes of Hines (1997) and Warner and McIntyre (1996, 2001) give comparable results.

3 Impacts on GCMs runs

3.1 Subgrid-scale orographic parameterization and lift

The model used in this study is a tropospheric version of the LMDz GCM (Hourdin et al. 2006). It is a gridpoint models, and in the simulation presented the gridpoints are regularly distributed in the longitude-latitude coordinates with resolution $3.75^0 \times 2.5^0$. The version used has 19 vertical sigma-levels unevenly spaced

to provide more resolution near the ground and in the lower stratosphere. In the experiment presented below, the different tunable parameters of the orographic forces scheme are: $H_{NC} = 1$, $C_d = 1$, $G = 1$, $\beta = 0.5$, $Ri_c = 0.25$ and $C_l = 1$. To perform simulations that can be compared to the observed climate, and to ensure that the results presented are significant, the model is integrated over long periods and forced with observed sea-surface temperatures and sea-ice distribution.

In different set of experiments discussed with some details in Lott 1998, where the different parts of the orography parameterization scheme were each tested independently, it was found that the low-level blocked flow drag improves the low-level flow, but slightly degrade the steady planetary wave. Similar results were found for the gravity wave part of the scheme: gravity waves drag improves the westerlies at the upper levels (Palmer et al., 1986) and at low levels where the trapped waves (Miller et al., 1989) reinforce the impact of the blocked drag. For the simulation of the steady planetary wave, the gravity waves drag is rather neutral, its impact is similar to that of the blocked flow drag. The lift scheme alone on the other hand appeared beneficial for the steady planetary wave, but does not affect the zonal wind very much.

The impact of the scheme on the model is represented on the differences map shown in Fig. (1) and Fig. (2). For both the zonal wind and the steady planetary wave it appears that the model is closer to the climatology with the orographic parameterization. The parameterized drag tends to reduce errors at nearly all levels on the zonal wind. The benefits of the scheme are nevertheless the greatest at low-levels (below $900hPa$) where the drag is maximum and at high-levels (above $100hPa$), where the parameterized gravity waves break. The steady planetary waves differences are also reduced nearly everywhere in the northern hemisphere, and particularly over the continents. Improvements are nevertheless more evident over North America where the scheme efficiently improves the simulation of the ridge over the rocky mountains. The scheme is also helpful for the simulation of the steady planetary wave over northern Europe and northern Asia, but it does not reduce the errors south and east of the Himalaya plateau.

3.2 Non-orographic gravity waves spectral parameterization

3.2.1 Zonal winds

In comparison with the essentially tropospheric LMD-GCM used in Section 3.1 the extended LMD-GCM to the middle atmosphere spans all heights ranging from the surface to 0.01 mb (approximately 80 km), discretized into 50 levels of varying

thickness (Lott et al. 2005). Layers are approximately 1.5 km thick between 10 km and 60 km and then increase to about 8 km in the last two upper levels. A simple Rayleigh drag sponge layer is employed in the four upper layer at z=3.5, 67.5, 72.5 and 81.25 km, with damping time constants equal 10 day^{-1}, 5 day^{-1}, 2.5 day^{-1} and 1.25 day^{-1} respectively. These Rayleigh-drags are applied to the non-zonal component of the flow only, to prevent large scale waves downward reflection at the upper boundary, without violating Downward control principles (Shepherd et al., 1996).

The impact of the Gravity wave drag scheme on the simulated MA circulation is evaluated by comparing two 5-years long (1993-1997) experiments, one with and the other without parameterized orographic and non-orographic gravity wave drag. The parameters used for the orographic gravity waves drag are the ones given in Section 3.1. The non-orographic Hines (1997) scheme is used with a low source strength, corresponding to an r.m.s. gravity- wave wind of 1.$m\ s^{-1}$ at the launch level. The launch level is the model ground.

Figure 3 shows the zonal mean wind in the model simulation in absence of gravity wave drag for four different months. In this case, the model shows the usual enormous westerly biases in the simulated winds at mid-latitude, and at nearly all levels above 20-30km (for a comparison with climatology see for instance Fig. 4 in Beagley et al. 1997). Figure 4 shows that these errors can be considerably reduced when introducing the gravity wave schemes, although discrepancies with observations still exist.

In the tropics, the reduction of the biases from one experiment to the other does not appear clearly in Figures 3 and 4, as differences between the two simulations are less pronounced in this region.

3.2.2 Tropical oscillations

For a finer analysis, it is conventional to look at a time-series of the zonal mean zonal wind at the equator as a function of height. Figure 5 shows such a picture for both simulations for the year 1993. A semi-annual oscillation is clearly evident in both model integrations at the tropopause (around 60-70 km), extending down to 45-50 km into the middle atmosphere. We note, however, that the westerly phase is too weak and does not descend far enough compared with observations (see for instance Hamilton and Mahlman, 1988). However, these defects are far more pronounced without Gravity waves drag (Figure 5a) than with gravity waves drag (Figure 5b). Furthermore, gravity waves also significantly reduce westerly biases.

The fact that explicit simulation of tropical oscillations (semi-annual oscillation and quasi-biennial oscillation) in general circulation models of the middle

atmosphere can be much improved by gravity waves drag parameterization is now illustrated. Because these oscillations need an accurate vertical resolution to be properly resolved, the simulations presented next are made with a version of the LMD-GCM that still include 50 vertical levels but with the upper boundary placed at 65km instead of 80km. Two simulations are made that differ from each other only in the source strength. In the first one (weak Hines), the source strength corresponds to a r.m.s. gravity-wave wind of $1.m\ s^{-1}$ at the ground while in the second one (strong Hines) it is $1.25m\ s^{-1}$.

Both simulations (Figure 6a and b) exhibit a semi-annual oscillation signal. However, the weak Hines experiment (Figure 6a) shows a westerly phase that does not go beyond 45 km, while in the strong Hines experiment it descends down to 35 km, which is in far better agreement with the observations. Below these levels (i.e., including the quasi-biennial oscillation domain) the model presents a systematic easterly bias, and nearly no seasonal and inter-annual oscillations. Note nevertheless, that with a strong Hines scheme and around 35-40 km, the adjacent westerly phase of the semi-annual oscillation near coalesces between January and July of the second year and between July of the year 3 and January of the year 4. This indicates that the model is near producing an inter-annual tropical oscillation. It is too small nevertheless to maintain itself and descend further below 35km.

Note here that our results are here in good part due to the fact that the vertical resolution of the model in the low and middle stratosphere is not sufficiently refined. Models with higher resolution and GWs parameterization can today reproduce a quite realistic QBO (Giorgetta et al. 2006).

4 Concluding remarks

During the 1990s, substantial progress was made in the understanding of the GWs generation by mountains as well as on the atmospheric general circulation. At almost the same time, it became clear that non-orographic gravity waves are also significant for the climate, if we look at it in the middle atmosphere. The gravity waves up there being much less predictible, they are parameterized using techniques that are essentially statistical.

With the development of the International Monitoring System for the enforcement of the Comprehensive Nuclear Test Ban Treaty, there is a challenge to gain a still better understanding of the role of gravity waves in infrasound propagation. The primary need is to identify conditions for which gravity waves can be expected and how they can be represented in propagation models. Although the asymptotic methods that are used by the geophysical community permit to explain some basic properties of infrasonic signals observed during experiments, a fresh look at

the problem starting with the GCM approach may prove to be fruitful. Both improvements of the parameterization of gravity waves and successful extensions of GCM to high altitudes make possible the use of GCM to locate the places where strong interactions between the acoustic disturbances and the atmospheric GWs can occur.

One of the most frustrating aspects of infrasound propagation research is our inability to predict the intensity of infrasonic arrivals. This follows that the acoustic waves are very sensitive to the state of the atmosphere, and becomes nonlinear for even moderate amplitudes. Recent progress in "computational aeroacoustics", through the class of dispersion-relation-preserving numerical schemes or shock-capturing numerical schemes, could provide tools for a rigorous approach to this problem. By considering suited constitutive equations, this approach can include the relaxation processes and the absorption due to shear and bulk viscosity. Such numerical schemes could be used in GCM to capture the long-range propagation of shock waves generated by a pulse.

Finally, the main difficulty is to match, in a consistent scheme, different numerical models valid in widely different ranges of spatial and temporal scales. With the advent of large parallel computing systems and high resolution data, the assimilation of microbarograph data to correct the infrasound propagation may soon become reality (see Part III in this book).

Beagley, S.R., J. de Grandpré, J.N. Koshyk, N.A. McFarlane and T.G. Shepherd, 1997: Radiative Dynamical climatology of the first generation Canadian middle atmosphere model, *Atmosphere Ocean*, **3**, 293–331.

Bougeault, P., A. Jansa, J. Attie, I. Beau, B. Benech, R. Benoit, P. Bessemoulin, J. Caccia, J. Campins, B. Carrissimo, J. Champeaux, M. Crochet, A. Druilhet, P. Durand, A. Elkhafi, P. Flamant, A. Genoves, M. Georgelin, K. Hoinka, V. Klaus, E. Koffi, V. Kotroni, C. Mazaudier, J. Pelon, M. Petitdidier, Y. Pointin, D. Puech, E. Richard, T. Satomura, J. Stein, and D. Tannhauser, 1993, The atmospheric momentum budget over a major mountain range: first results of the PYREX field program, *Annales Geophysicae*, *11*, 395–418, 1993.

Clark, T. L., and W. R. Peltier, 1984, Critical level reflection and the resonant growth of nonlinear mountain waves, *J. Atmos. Sci.*, *41*, 3122–3134, 1984.

Dalaudier, F., Sidi, C., Crochet, M., Vernin, J., 1994, Direct evidence of "sheets" in the atmospheric temperature field, *J. Atmos. Sci.*, *51*, 237–248, 1994.

D'Andrea, F., S. Tibaldi, M. Blackburn, G. Boer, M. Déqué, M. Dix, B. Dugas, L. Ferranti, T. Iwasaki, A. Kitoh, V. Pope, D. Randall, E. Roeckner, D. Sraus,

W. Stern, H. van der Dool, and D. Williamson, 1996, Northern hemisphere atmospheric blocking as simulated by 15 atmospheric general circulation models in the period 1979-1988, *Climate Dynamics*, *Submitted*, 1996.

Durran, D. R., 1987, Another look at downslope winds. Part 2: Nonlinear amplification beneath wave-overturning layers, *J. Atmos. Sci.*, *44*, 3402–3412, 1987.

Fritts, D. C. and Dunkerton, T. J., 1984, A quasi-linear study of gravity wave saturation and self-acceleration, *J. Atmos. Sci.*, **41**, 3272–3289, 1984.

Giorgetta, M.A, E. Manzini, E. Roeckner, M. Esch, and L. Bengston, 2006: Climatology and forcing of the quasi-biennial oscillation in the MAECHAM5 model, *Journal of Climate,* **19,** 3882-3901.

Hamilton, K. and J.D. Mahlman, 1988: General Circulation Model simulation of the semi-annual oscillation of the tropical middle atmosphere. *J. Atmos. Sci.*, **45**, 3212-3235.

Held, I. M., Stationary and quasi-stationary eddies in the extratropical troposphere: Theory, *Large-scale Dynamical Processes in the Atmosphere,* B. J. Hoskins and R. P. Pearce, Eds., Academic Press, London, 397pp.

Hines, C. O., 1997, Doppler-spread parameterization of gravity wave momentum deposit in the middle atmosphere. Part 2: Broad and quasi-monochromatic spectra and implementation, *J. Atmos. Solar-Terrest. Phys.*, **59**, 387–400.

Hourdin, F., I. Musat, S. Bony, P. Braconnot, F. Codron, J.-L. Dufresne, L. Fairhead, M.-A. Filiberti, P. Friedlingstein, J.-Y. Grandpeix, G. Krinner, P. Levan, and F. Lott, The LMDZ4 general circulation model: climate performance and sensitivity to parametrized physics with emphasis on tropical convection,*Climate Dynamics,* **27,** 787-813,DOI: 10.1007/s00382-006-0158-0 , 2006.

Kulichkov S. N., Avilov K. V., Bush G. A., Popov O. E., Raspopov O. M., Baryshnikov A. K., Re Velle D. O. and Whitaker R. W., 2004, On anomalously fast infrasonic arrivals at long distances from surface explosions, *Izvestiya, Atmospheric and Oceanic Physics*, *40*(1), 1–9.

Kulichkov S. N., Avilov K. V., Popov O. E., Otrezov A. I., Bush G. A. and Baryshnikov A. K., 2004, Some results of simulation of long-range infrasonic propagation in the atmosphere, *Izvestiya, Atmospheric and Oceanic Physics*, *40*(2), 202–215.

Kulichkov S. N., Bush G. A. and Svertilov A. I., 2002, New type of infrasonic arrivals in the geometric shadow region at long distances from explosions (2002), *Izvestiya, Atmospheric and Oceanic Physics*, *38*(4), 397–402.

Lindzen, R. S., 1981, Turbulence and stress due to gravity waves and tidal breakdown, *J. Geophys. Res.*, **86**, 9707–9714.

Lott, F., and M. Miller, 1997, A new subgrid scale orographic drag parameterization; its testing in the ECMWF model, *Q. J. Roy. Meteorol. Soc.*, *123*, 101–127, 1997.

Lott, F., 1995, Comparison between the orographic response of the ECMWF model and the PYREX 1990 data, *Q. J. Roy. Meteorol. Soc.*, *121*, 1323–1348, 1995.

Lott, F., 1998, Linear mountain drag and averaged pseudo momentum profiles in the presence of trapped lee waves, *Tellus*, **50A**, 12–25.

Lott, F., 1999, Alleviation of stationary biases in a GCM through a mountain drag parameterization scheme and a simple representation of mountain lift forces, *Monthly Weather Review*, **127**, 788–801.

Lott, F.,L. Fairhead, F. Hourdin and P. Levan, 2005, The stratospheric version of LMDz: Dynamical Climatologies, Arctic Oscillation, and Impact on the Surface Climate. *Climate Dynamics*, **25,** 851-868, DOI: 10.1007/s00382-005-0064-x.

Manzini, E., N.A. McFarlane, and C. McLandress, 1997, Impact of the Doppler Spread Parameterization on the simulation of the middle atmosphere circulation using the MA/ECHAM4 general circulation model, *J.Geophys. Res.*, **102**, 25751-25762.

Miller, M. J., T. N. Palmer, and R. Swinbank, 1989, Parametrization and influence of subgridscale orography in general circulation and numerical weather prediction models, *Meteorology and Atmospheric Physics*, *40*, 84–109, 1989.

Millet, C., Robinet J. C., and Roblin, C., 2007, On using computational aeroacoustics for long-range propagation of infrasounds in realistic atmospheres, *Geophys. Res. Letters*, **34**, 2007.

Miranda, P. M. A., and I. A. James, 1992, Non-linear three dimensional effects on gravity-wave drag: splitting flow and breaking waves, *Q. J. Roy. Meteorol. Soc.*, *118*, 1057–1081, 1992.

Palmer, T. N., G. J. Shutts, and R. Swinbank, 1986, Alleviation of systematic westerly bias in general circulation and numerical weather prediction models through an orographic gravity wave drag parameterization, *Q. J. Roy. Meteorol. Soc.*, *112*, 2056–2066, 1986.

Ponomarev E. A., Rudenko G. V., Sorokin A. G., Dmitrienko I. S., Lobycheva I.Y. and Baryshnikov A. K., 2006, Using the normal-mode method of probing the infrasonic propagation for purposes of the comprehensive nuclear-test-ban-treaty, *68*, 599–614, 2006.

Schär, C., and D. R. Durran, 1996, Vortex formation and vortex shedding in continuously stratified flows past isolated topography, *J. Atmos. Sci.*, *54*, 534–554, 1996.

Shepherd, T.G., K. Semeniuck and J.N. Koshyck, 1996: Sponge layer feedback in middle atmosphere models. *J. Geophys. Res.*, **101**, 23,447–23,464.

Smith, R. B., 1979, Some aspects of the quasi-geostrophic flow over mountain, *J. Atmos. Sci.*, *36*, 2385–2393, 1979.

Stephenson, D. B., 1994, The northern hemisphere tropospheric response to changes in the gravity-wave drag scheme in a perpetual January GCM., *Q. J. Roy. Meteorol. Soc.*, *120*, 699–712, 1994.

Warner, C. D. and Mc Intyre, M. E., 1996: On the propagation and dissipation of gravity wave spectra through a realistic middle atmosphere. *J. Atmos. Sci.*, **53**, 3213–3235.

Warner, C. D. and Mc Intyre, M. E., 2001: An ultra-simple spectral Spectral Parameterization for Nonorographic Gravity Waves, *J. Atmos. Sci.*, **58,** 1837-1857.

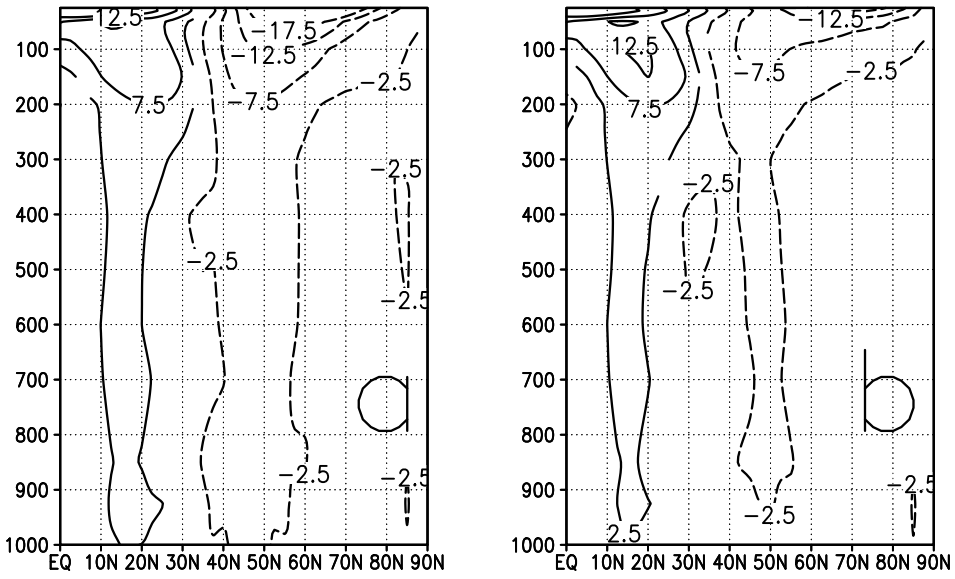

Figure 1: Difference between the zonal wind of the NMC analysis and that of the G CM simulations: DJF 85-93. Zero line not shown, negative values are dashed. (a) C ontrol run; (b) run with parameterization.

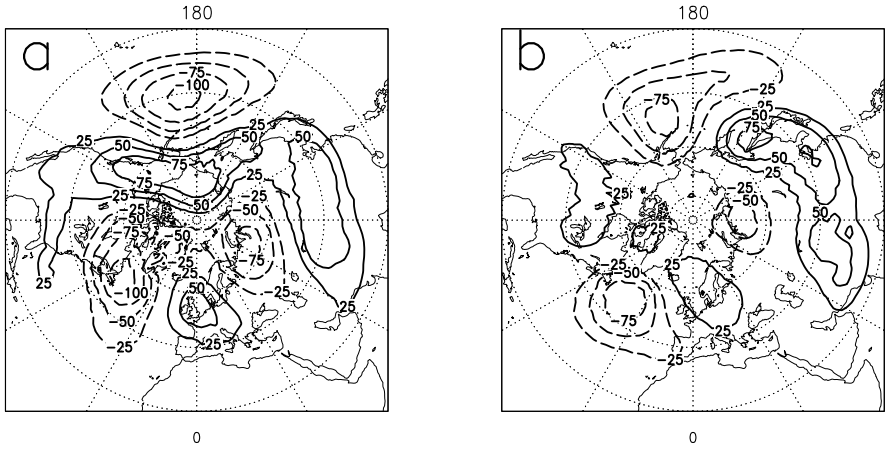

Figure 2: Difference between the Geopotential height anomaly at $500hPa$ of the NMC analysis fields and that of the GCM simulations: DJF 85-93. Zero line not shown, negative values are dashed. (a) Control run; (b) run with parameterization.

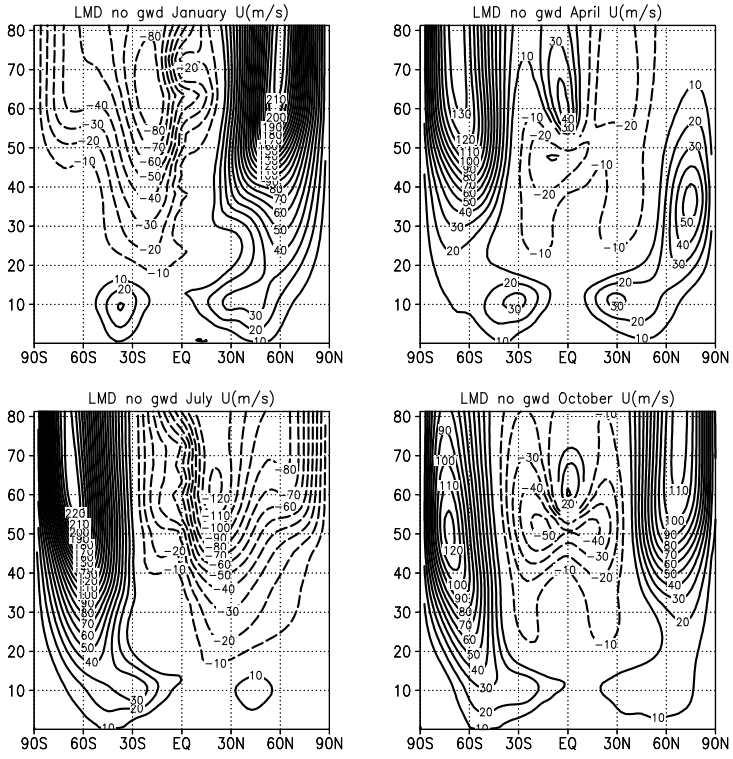

Figure 3: Zonally averaged zonal wind field calculated from a 5-year run of the LMD-GCM with no gravity wave drag. Contour interval = 10 m/s, negative values are dashed

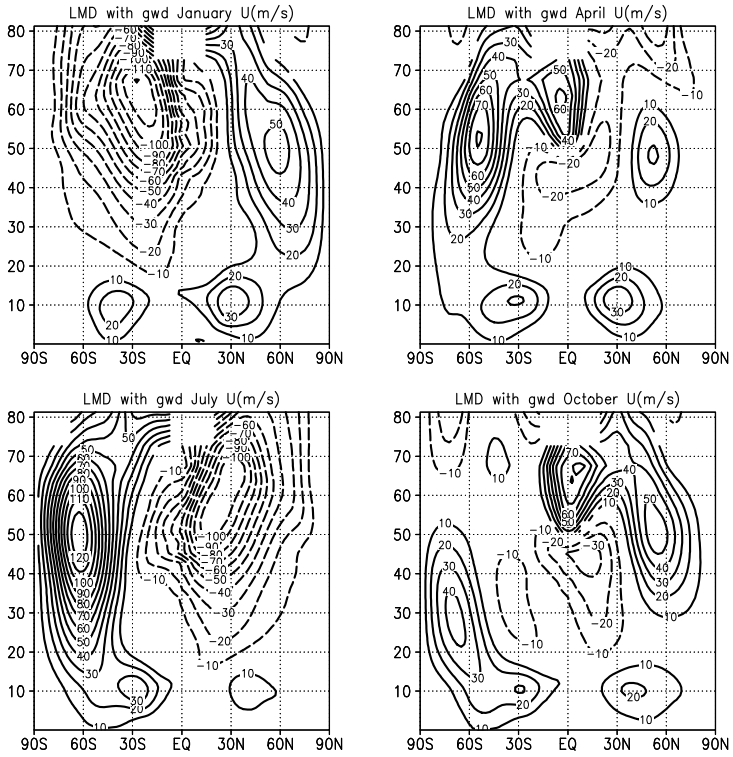

Figure 4: Zonally averaged zonal wind field calculated from a 5-year run of the LMD-GCM with both non-orographic (Hines) and orographic (Lott and Miller) gravity waves drag included. Contour interval = 10 m/s, negative values are dashed

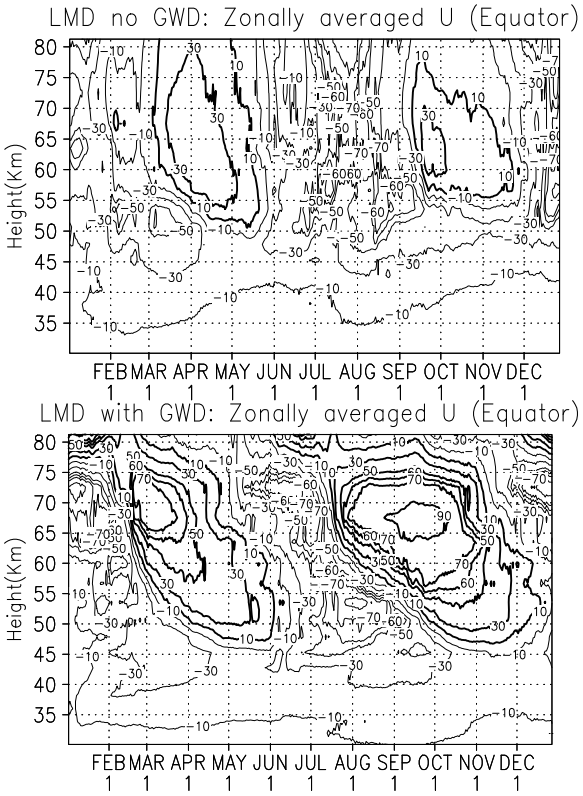

Figure 5: a) March of zonally averaged zonal wind at the equator for the year 1993 of the LMD-GCM integrations without gravity waves drag. b) As a) but for the integration with gravity waves drag. Contour interval = 20 m/s in both panels. Positive values are thick solid, nagative values are thin solid.

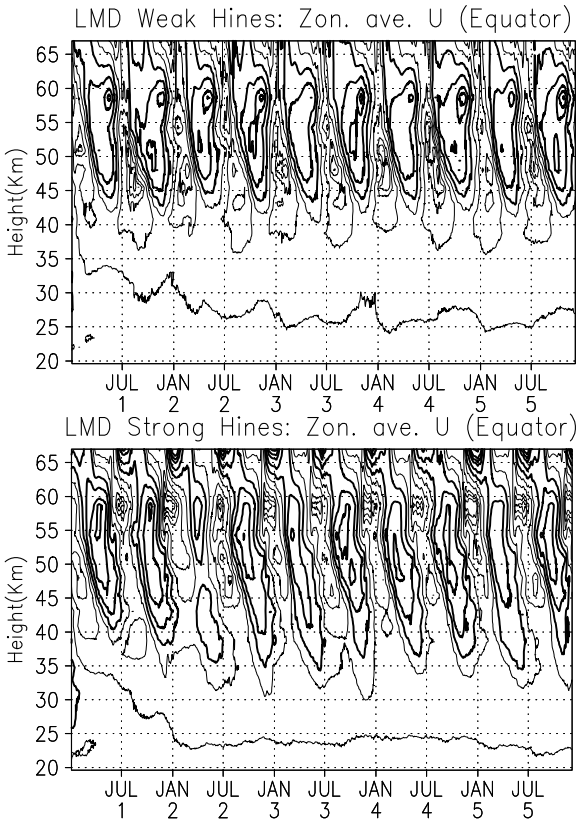

Figure 6: a) March of zonally averaged zonal wind at the equator for the period 1993-97 of the LMD-GCM integrations with gravity waves drag. b) As a) but for a stronger gravity waves forcing. Contour as in Figure 5.